

ULTRAVIOLET LIGHT CURVES OF SUPERNOVAE WITH THE *SWIFT* ULTRAVIOLET/OPTICAL TELESCOPE

PETER J. BROWN¹, STEPHEN T. HOLLAND^{2,3,4}, STEFAN IMMLER^{2,4}, PETER MILNE⁵, PETER W. A. ROMING¹, NEIL GEHRELS², JOHN NOUSEK¹, NINO PANAGIA^{6,7,8}, MARTIN STILL⁹, AND DANIEL VANDEN BERK¹

¹ Pennsylvania State University, Department of Astronomy & Astrophysics, University Park, PA 16802, USA

² Astrophysics Science Division, Code 660.1, NASA/Goddard Space Flight Center, Greenbelt, MD 20770, USA

³ Universities Space Research Association, 10227 Wincopin Circle, Suite 221, Columbia, MD 21044, USA

⁴ Centre for Research and Exploration in Space Science and Technology Code 660.8, NASA/GSFC, Greenbelt, MD 20770, USA

⁵ Steward Observatory, University of Arizona, 933 North Cherry Avenue, Tucson, AZ 85721, USA

⁶ Space Telescope Science Institute, 3700 San Martin Drive, Baltimore, MD 21218, USA

⁷ INAF-Osservatorio Astrofisico di Catania, Via S. Sofia 78, I-95128 Catania, Italy

⁸ Supernova Ltd., OYV #131, Northsound Road, Virgin Gorda, British Virgin Islands

⁹ Mullard Space Science Laboratory, Department of Space and Climate Physics, University College London, Holmbury St. Mary, Dorking, Surrey, RH5 6NT, UK

Received 2008 March 8; accepted 2009 February 12; published 2009 April 7

ABSTRACT

We present ultraviolet (UV) observations of supernovae (SNe) obtained with the UltraViolet/Optical Telescope (UVOT) on board the *Swift* spacecraft. This is the largest sample of UV light curves from any single instrument and covers all major SN types and most subtypes. The UV light curves of SNe Ia are fairly homogenous, while SNe Ib/c and IIP show more variety in their light-curve shapes. The UV-optical colors clearly differentiate SNe Ia and IIP, particularly at early times. The color evolution of SNe IIP, however, makes their colors similar to SNe Ia at about 20 days after explosion. SNe Ib/c are shown to have varied UV-optical colors. The use of UV colors to help type SNe will be important for high-redshift SNe discovered in optical observations. These data can be added to ground-based optical and near infrared data to create bolometric light curves of individual objects and as checks on generic bolometric corrections used in the absence of UV data. This sample can also be compared with rest-frame UV observations of high-redshift SNe observed at optical wavelengths.

Key words: distance scale – dust, extinction – galaxies: distances and redshifts – supernovae: general – ultraviolet: general

Online-only material: color figures, extended figure, machine-readable and VO tables

1. ULTRAVIOLET SUPERNOVA OBSERVATIONS

From the earliest photon signal from a supernova (SN) during the shock breakout, the UV light from SNe contains many clues about the explosion and the environment, with application to both nearby and high-redshift SNe. The contribution of UV light to the bolometric luminosity can be significant, particularly at the earliest epochs when the high temperature yields a large UV flux. Because line blanketing in the UV is dominated by iron peak elements, the UV brightness is sensitive to the ionization level (see Dessart et al. 2008) and differences in metallicity (Nugent et al. 1997; Lentz et al. 2000; Sauer et al. 2008). The large UV extinction observed in most extinction curves also allows UV observations to better constrain the reddening to individual objects (Jeffery et al. 1994).

The first observation of UV light from an SN was performed by the Orbiting Astronomical Observatory in 1972, revealing the UV faintness of a type I SN (Holm et al. 1974). The *International Ultraviolet Explorer* (*IUE*) built up a larger sample with UV spectroscopic observations of 25 SNe (Cappellaro et al. 1995), with excellent light curves for Ia IIL 1979C (Panagia et al. 1980) and 1980K, the Ib 1983N, Ia 1992A (Kirshner et al. 1993), as well as the II-pec 1987A (Kirshner et al. 1987; Pun et al. 1995). The spectacular event of SN 1987A was also observed in the UV by the Astron Station (Lyubimkov 1990). The *Hubble Space Telescope* (*HST*) has added excellent UV spectroscopic and photometric data for another ~30 SNe (Wang et al. 2005; see also Panagia 2003 for a review of *IUE* and *HST* UV observations up to that time). The Galaxy Evolution Explorer and the Optical Monitor on the *XMM-Newton* mission have also observed SNe

in the UV (Gal-Yam et al. 2008; Immler et al. 2005). Rest-frame UV observations of higher redshift SNe observed in the optical from the ground are also now being regularly obtained (Astier et al. 2006; Foley et al. 2008; Ellis et al. 2008).

The latest UV observatory is the *Swift* UVOT (Romig et al. 2005). The *Swift* observatory's quick response capability and short term scheduling, necessitated by the unpredictable and variable behavior of individual gamma-ray bursts (GRB), also allows newly discovered SNe to be observed quickly and with well sampled light curves (Gehrels et al. 2004). Data are available in a matter of hours, and observing times and filter combinations can be changed on a day-to-day basis depending on what is seen in recent observations. Thus far, *Swift* has focused on nearby SNe ($z \lesssim 0.02$) for which high quality data can be obtained with only a small impact on spacecraft operations and *Swift*'s primary mission to detect and observe GRBs. SN observations are performed under *Swift*'s Target of Opportunity (ToO) program.¹⁰ A dedicated Web site¹¹ has been set up that gives the status of *Swift* SN observations, images and regularly updated light curves for the benefit of the community.

In this paper, we present some of the overall UV properties of SNe seen in our sample. In particular, we contrast the UV light-curve shapes and colors of the different types, which is best done with a sample observed with the same instrumental setup. Understanding the brightness (relative to the optical) and temporal behavior should assist future observatories to

¹⁰ <http://www.swift.psu.edu/too.html>.

¹¹ see http://swift.gsfc.nasa.gov/docs/swift/sne/swift_sn.html.

Table 1
Swift UVOT Filter Characteristics

Filter	λ_{central} (Å)	FWHM (Å)	Zero Point (mag)
<i>uvw2</i>	1928	657	17.35 ± 0.03
<i>uvm2</i>	2246	498	16.82 ± 0.03
<i>uvw1</i>	2600	693	17.49 ± 0.03
<i>u</i>	3465	785	18.34 ± 0.020
<i>b</i>	4392	975	19.11 ± 0.016
<i>v</i>	5468	769	17.89 ± 0.013

understand the sampling and depth necessary to characterize a UV light curve.

2. OBSERVATION SUMMARY

The *Swift* UVOT has observed 45 SNe (21 Ia, 13 Ib/c, and 11 II) between 2005 March (Brown et al. 2005) and 2007 August. SNe chosen for observation by *Swift* are generally young and nearby ($z < 0.02$), and should be offset from bright field stars or the host galaxy nucleus by at least $\sim 10''$. Low extinction is also preferred, particularly for more distant SNe, though a few nearby events (notably SNe 2006X, 2006bp, and 2007bm) do suffer from significant extinction. These criteria have been dynamically evolving as a result of experience and are less strictly applied for rarer events. Thus we are not an unbiased sample but strive to observe the range of SN events accessible to the UVOT.

The UVOT typically observes SNe with three UV and three optical broadband filters. The central wavelengths and widths are given in Table 1 (Poole et al. 2008). Brown et al. (2007b) display the transmission of these filters with respect to SNe spectra. The UVOT also has low-resolution spectroscopic grisms. However, like *IUE*, UVOT grism spectra are limited to the brightest epochs of the nearest SNe. Here we focus on results from the photometry; spectroscopic results will be presented elsewhere (Bufano et al. 2009).

Images were obtained from the *Swift* archive, and for those whose most recent processing occurred prior to 2007, the raw images and event lists were reprocessed, primarily to utilize an improved plate scale for the *uvw2* images and corrections to exposure times in the headers. Exposures were aspect corrected then coadded by epoch, usually corresponding to unique observation numbers. Due to the rapid evolution of SN 2006aj/GRB060218 during the two days the exposures in the first two observation segments were coadded into subepochs and subsequent observations coadded by day as usual.

We performed aperture photometry using a $3''$ source aperture, similar in size to the UVOT point-spread function (PSF), to improve the signal to noise and minimize the amount of galaxy contamination that must be subtracted (and the corresponding error) compared to larger apertures (see Li et al. 2006). In each frame we measured the background using a region separated from the galaxy that is free of stars. Counts within a $5''$ aperture centered on the SN were used to compute the coincidence loss correction factor (to be consistent with the instrument calibration). Only for the optical data of SN 2005df is the source count rate too high to confidently correct for coincidence loss. The galaxy count rate was measured using the same aperture and background region in template images obtained before or well after the SN explosion. In addition to the Poisson errors, an additional 3% uncertainty was added in quadrature to account for large and small scale variations within the center of the UVOT

detector (Poole et al. 2008). An example of the count rate light curve is shown in the left panel of Figure 1. The galaxy count rate was subtracted from the count rate of the SN+galaxy measured in the SN images, following which an average PSF for each filter was used to compute the aperture correction factor for the count rates from our $3''$ aperture to the $5''$ for which the zero points are calibrated (Poole et al. 2008). We have used this method instead of the typical image subtraction so that the effect of coincidence loss can be accounted for in the individual images before subtraction. For SNe well below the coincidence loss limit and with a low galaxy background standard image subtraction can give good results (Modjaz et al. 2008). Since the coincidence loss correction was calibrated for point sources, it becomes less accurate at higher background rates. Based on comparisons with ground based *BV* data, the error in the coincidence loss correction is negligible at 4.4 counts s^{-1} (SN 2006X *b* data compared to Wang et al. 2008 in the right panel of Figure 1), increasing to 0.1 mag at 7.8 counts s^{-1} (SN 2005cs *v* data compared to ground-based data in Dessart et al. 2008). For this paper, we set a limit of 6 counts s^{-1} above which we do not report the data here pending further analysis. Five SNe in our sample have optical count rates higher than this—SNe 2005cs, 2006bc, 2006dd, 2006mr, and 2007bm. In addition the presence of a nearby star interferes with the coincidence loss correction for the optical data of SN 2005am which is also excluded here. In most cases, the UV count rates are a factor of ~ 10 lower and are not affected. The UVOT photometry for the 25 SNe is given in Table 2. These light curves are based on the new calibration (affecting primarily the *UV* magnitudes) and supercedes the photometry from Brown et al. (2005), Immler et al. (2006), Immler et al. (2007), and Brown et al. (2007a). The optical *bv* light curves are consistent with available ground-based data (see Phillips et al. 2007; Wang et al. 2008, 2009) except those listed above for which the coincidence loss correction is uncertain.¹²

From our observations of 45 SNe, the light curves of 25 SNe (17 Ia, 3 Ib/c, and 5 II) with at least three UV detections above 3σ (accounting for Poisson errors in the SN and galaxy count rates) are displayed on a continuous timeline in Figure 2. Figure 2 illustrates the dynamic range and frequency of *Swift* SN observations. The bright limit, above which coincidence losses are hard to correct, is approximately 12th magnitude in the UV. In practice, this saturation limit from a bright SN or an SN on a bright galaxy background has affected the optical light curves of some of these SNe but not the UV light curves. The faint limit can be as deep as about 21 mag (depending on the depth of the SN and template observations) but observations are typically terminated once the galaxy light dominates within the aperture.

In order to easily contrast the light curves of the different SN types, Figure 3(a) shows the UVOT light curves of a well observed example of each type, with light curves of the individual SNe displayed in Figures 3(b)–(z) in the electronic edition. For easy comparison, the time and magnitude axis are the same scale across the plots and the magnitudes are unshifted to show the relative colors.

3. LIGHT CURVES

The temporal behavior of the UV light varies with SN type. Figure 4 shows the UV light curves for the SNe grouped by type and shifted in magnitude for comparison of the early shapes. To determine the explosion date we have assumed a rise time of

¹² The UVOT *u* band is not compared with ground-based *U* filters since the UVOT filter has considerable transmission blueward of ground-based filters.

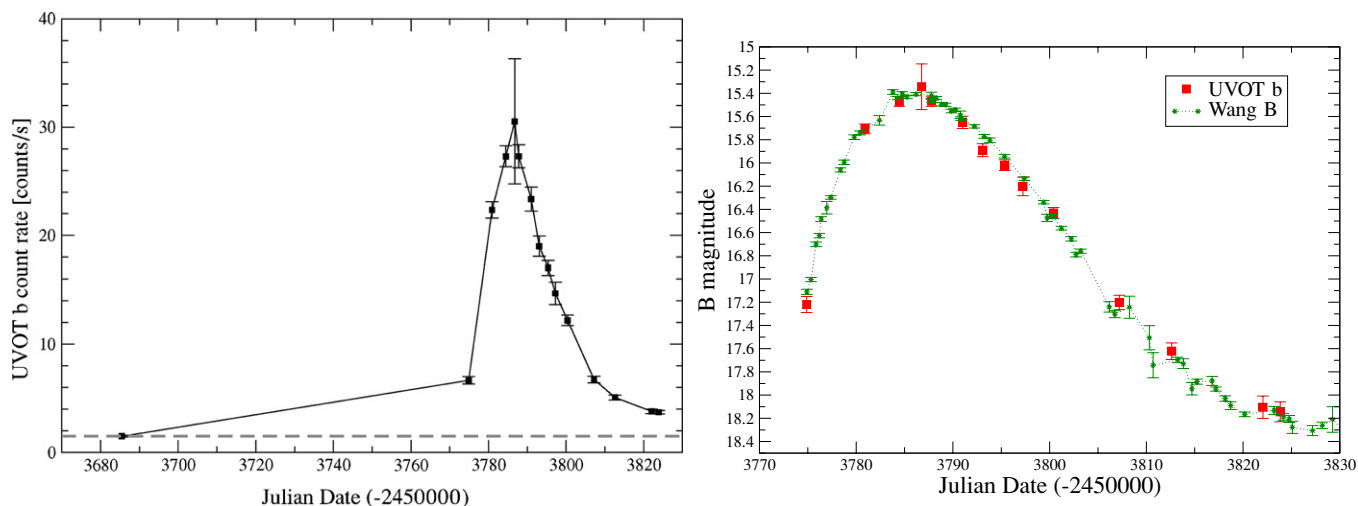


Figure 1. Left panel: background subtracted and coincidence loss corrected count rates in a $3''$ aperture at the location of SN 2006X before and after explosion. The galaxy count rate measured before the explosion (shown as a dotted line in the figure) is subtracted from the later observations to give the SN count rate. Right panel: comparison of the UVOT b -band light curve, measured in a $3''$ aperture with the galaxy count rate subtracted, compared to the B -band data in (Wang et al. 2009).

(A color version of this figure is available in the online journal.)

Table 2
SN Light Curves

SN name	filter	JD (-2,450,000)	mag (mag)	err (mag)
SN2007aa	<i>uvw2</i>	4156.25	19.75	0.26
SN2007aa	<i>uvw2</i>	4162.36	NULL	19.79
SN2007aa	<i>uvw2</i>	4168.43	NULL	20.06
SN2007aa	<i>uvw2</i>	4184.94	NULL	20.34
SN2007aa	<i>uvm2</i>	4156.22	NULL	19.73
SN2007aa	<i>uvm2</i>	4168.44	NULL	19.91
SN2007aa	<i>uvm2</i>	4184.94	NULL	20.07
SN2007aa	<i>uvw1</i>	4156.24	18.55	0.13
SN2007aa	<i>uvw1</i>	4160.87	18.95	0.16
SN2007aa	<i>uvw1</i>	4162.36	18.62	0.19
SN2007aa	<i>uvw1</i>	4168.45	19.35	0.23
SN2007aa	<i>uvw1</i>	4179.61	19.89	0.30
SN2007aa	<i>uvw1</i>	4184.93	19.46	0.22
SN2007aa	<i>u</i>	4156.25	16.91	0.06
SN2007aa	<i>u</i>	4179.62	18.02	0.09
SN2007aa	<i>u</i>	4184.93	17.90	0.08
SN2007aa	<i>b</i>	4156.25	16.39	0.05
SN2007aa	<i>b</i>	4179.62	16.70	0.05
SN2007aa	<i>b</i>	4184.93	16.69	0.05
SN2007aa	<i>v</i>	4156.25	15.86	0.05
SN2007aa	<i>v</i>	4179.62	15.80	0.05
SN2007aa	<i>v</i>	4184.94	15.75	0.05

Notes. Upper limits are indicated by a “NULL” in the magnitude column and the 3σ upper limit in the error column. Errors given include the poisson errors in the SN and galaxy count rate measurements added in quadrature. Photometry for the full SN sample is included in the electronic version.

(This table is available in its entirety in machine-readable and Virtual Observatory (VO) forms in the online journal. A portion is shown here for guidance regarding its form and content.)

18 days to the maximum light in the V band for SNe Ia/b/c (Garg et al. 2007) expect for SN 2006aj for which we use the GRB trigger time from Campana et al. (2006). For the SNe II we use the explosion times determined by Dessart et al. (2008) for SNe 2005cs and 2006bp and estimate the others based on discovery and non-detection times in the discovery announcements. The light curves will be discussed in more detail by SN type below.

For a simple parameterization of the light-curve shape for comparison within and between SN types, we have chosen to measure the early decay rates in magnitudes per 100 days, corresponding to the parameter β in Pskovskii (1967). Multiple values of the early decay slope were measured from different ranges of early data points. In Table 3 we report the we report the midpoint between the upper and lower values and the range of magnitudes above and below the central value corresponding to flatter or steeper slopes. The range about the central decay rate is given, as using different subsections of the data can give steeper or shallower results depending on the quality of the data and the shape of the light curve, which is not necessarily linear. Histograms of these slopes are shown in Figure 5.

3.1. SNe Ia Light Curves

SNe Ia rise to a maximum in the UV peaking just before the optical. As seen in Figure 4 and similar to the optical, the UV brightness decays first steeply and then shallower due to radioactive decay of Nickel and Cobalt. The *uvw2* and *uvw1* light curves of SNe Ia are fairly uniform, and the *uvw1* curves match well with the *HST/IUE* spectrophotometry of SN 1992A in the comparable F275W band (Kirshner et al. 1993; Brown et al. 2005; Milne et al. 2007). The *uvm2* photometry is much fainter than the other bands, so the points have larger errors, but the light curves seem to exhibit different behavior—both in the time of the *uvm2* maximum and the shape of the light-curve decay. This is also reflected in the histograms in Figure 5, which reinforces this idea that the *uvw1* light curves of SNe Ia occupy a narrow range of decay rates compared to the other filters. The later shallow decay, γ in Pskovskii (1967), is only measurable for a few SNe Ia, notably SN 2006E which had a decay rate of about 2.2, 3.9, and 3.2 mag/100 days in *uvw1*, *uvm2*, and *uvw2*, respectively. More details on the light curves of SNe Ia and generation of UV light-curve templates will be presented in P. Milne et al. (2009, in preparation).

From a sample of light curves one can begin to discern what is normal and what is peculiar behavior. Two SNe Ia that stand out are SNe 2005hk and 2005ke. SN 2005hk was bluer than other SNe Ia and already fading in the UV when *Swift*

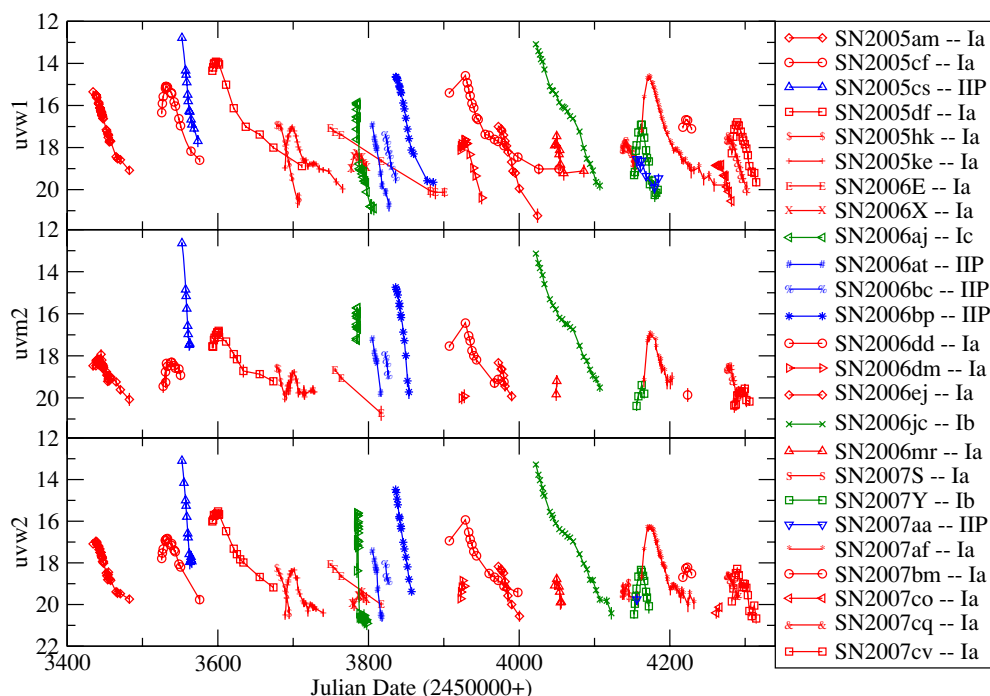


Figure 2. UV light curves of SNe detected in at least three epochs by the UVOT. In the online color version SNe Ia are displayed in red, SNe Ib/c in green, and SNe II in blue.

(A color version of this figure is available in the online journal.)

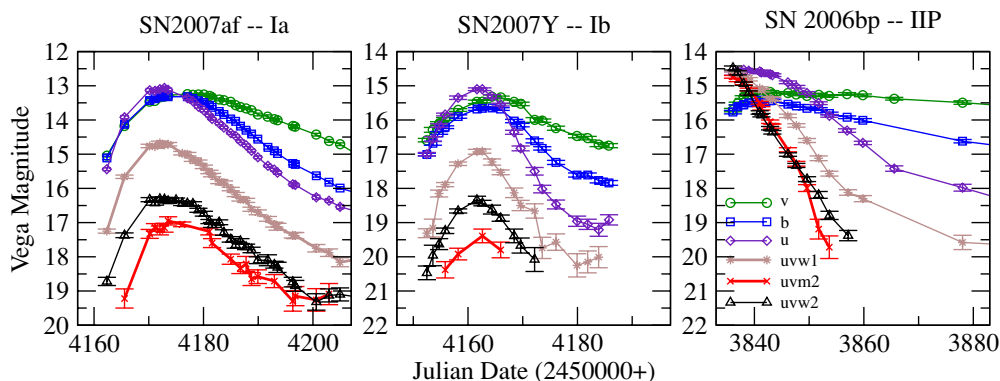


Figure 3. UVOT light curves of SN2007af, 2007Y, 2006bp. The time axis begins with the estimated explosion dates for SNe 2007af and 2007Y assuming a rise time of 18 days to the maximum light in the *V* band for SNe Ia/b/c (Garg et al. 2007; Stritzinger et al. 2002), while SN 2006bp uses the explosion date determined by Dessart et al. (2008). Individual light curves of all our SNe are available in the electronic version.

(An extended color figure is available in the online journal)

observations began, nearly 10 days before the optical maximum. SN 2005ke followed the typical Ia decay until about 15 days after maximum light when the UV brightness remained nearly constant for ~ 20 days before fading again. In conjunction with a marginal X-ray detection, this plateau in the UV light curves has been attributed to interaction with the circumstellar material (Immler et al. 2006), though other causes such as reduced line blanketing have been suggested (Kasliwal et al. 2008). SNe 2007ax (Kasliwal et al. 2008) and 2006mr show hints of extended emission at late times and this may be common behavior for subluminal SNe Ia.

3.2. SNe Ib/c Light Curves

For SNe Ib/c, the sample of well observed SNe is much smaller, with three light curves in our sample, but they appear to be as diverse in the UV as they are in the optical (see Figure 4).

Other SNe Ib/c were also observed but for only a single epoch or were not well detected (see Holland et al. 2007 for additional SNe Ib/c observed during *Swift*'s first two years). It is hard to define a generic UV behavior, so instead we briefly describe each well sampled SN.

SN 2006aj, a Ic SN, was discovered following *Swift* BAT trigger on GRB060218 (Campana et al. 2006). The UV initially rose rapidly reaching a bright peak about half a day after the trigger. This first peak has been attributed to the shock breakout from a dense stellar wind (Campana et al. 2006; Blustin 2007; Waxman et al. 2007) or self-absorbed synchrotron radiation (Ghisellini et al. 2007). This faded rapidly in the UV, plateauing briefly from 4–10 days after the explosion in *uvw2* and *uvw1*, after the trigger as the radioactive decay powered an SN light curve, and then faded again. In *uvm2* the SN was undetected at least 5 mag fainter than the earlier peak, showing the contrast between the UV bright shock and the UV faint SN

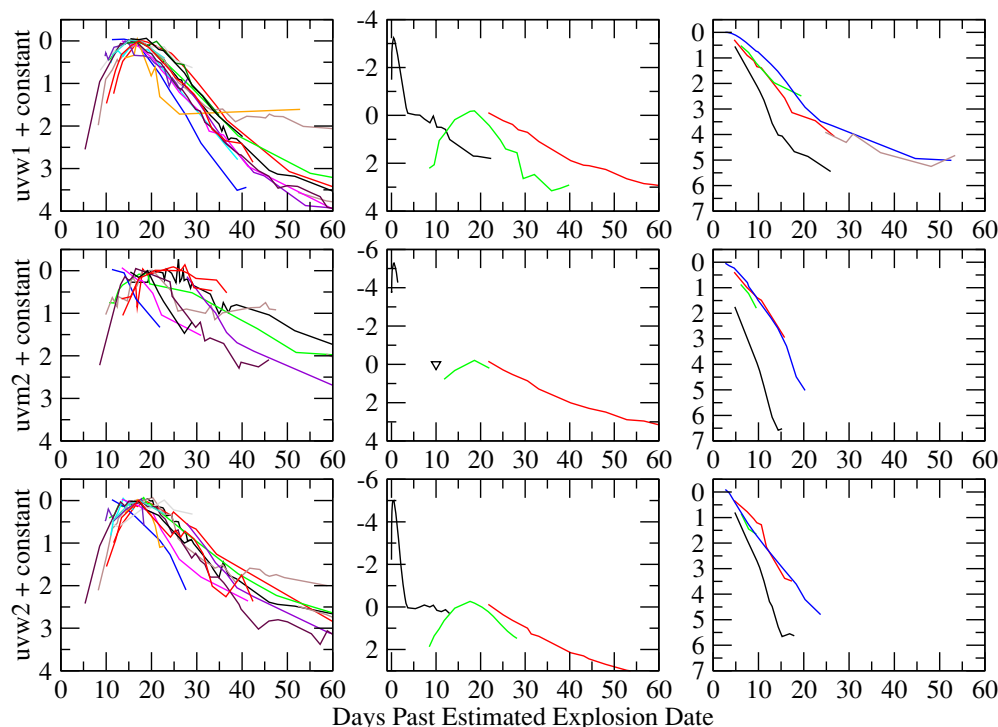


Figure 4. UV light curves of the SNe grouped by type. The time axis is determined by the estimated explosion date and the magnitudes shifted by subtracting the measured or estimated maximum magnitude. For SN 2006aj we have done the scaling based on the peak (for *uvw2* the deepest upper limit is marked with a downward triangle) of the radioactively powered portion of the SN light curve (rather than the bright, early shock) since that is the part of the light curve observed for the other Ib/c cases. The error bars are not displayed for a clearer comparison of the light-curve shapes.

(A color version of this figure is available in the online journal.)

Table 3
Decay Rates of Early UV Light Curves

SN Name	Type	<i>uvw1</i>	range	<i>uvw2</i>	range	<i>uvw2</i>	range
SN2005am	Ia	12.2	0.2	5.5	0.6	8.9	1.5
SN2005cf	Ia	12.2	1.3	4.1	0.8	8.2	1.2
SN2005cs	II	39.8	4.1	54.1	4.7	47.0	3.0
SN2005df	Ia	9.5	1.2	5.6	0.4	7.8	0.5
SN2005hk	Ia	16.4	1.3	14.6	1.0	12.0	1.8
SN2005ke	Ia	12.6	1.8	14.9	1.3	10.7	0.5
SN2006E	Ia
SN2006X	Ia	6.3	1.3
SN2006aj	Ic	14.1	4.0
SN2006at	II	20.0	2.4	20.8	2.0	22.1	5.6
SN2006bc	II	17.3	2.1	26.5	0.7	24.1	12.4
SN2006bp	II	16.4	2.9	23.8	2.1	26.0	1.4
SN2006dd	Ia	13.6	0.8	13.0	0.5	13.5	0.2
SN2006dm	Ia	12.7	0.3
SN2006ej	Ia	12.3	0.7	15.4	3.4	16.3	2.1
SN2006jc	Ib	9.9	1.0	10.2	1.5	11.6	1.4
SN2006mr	Ia	16.0	2.9
SN2007S	Ia	6.7	0.5
SN2007Y	Ib	20.0	1.7	18.1	1.3
SN2007aa	II
SN2007af	Ia	11.7	1.5	11.0	1.0	11.7	0.2
SN2007bm	Ia
SN2007co	Ia	13.2	0.3
SN2007cq	Ia	12.2	0.5	14.9	3.0	7.4	0.9
SN2007cv	Ia	12.0	1.0	8.5	0.8

Notes. Decay rates for the different filters are given in units of magnitudes per 100 days. Upper and lower values of the early decay slope were measured from different ranges of early data points. Here we report the midpoint and the range of magnitudes above and below the central value corresponding to flatter or steeper slopes.

component. The optical curves are consistent with an SN Ic of intermediate luminosity between normal SNe Ic and previous GRB-associated, overluminous SNe Ic (see Pian et al. 2006 and Modjaz et al. 2006).

SN 2006jc was a peculiarly bright and blue SN Ib (Foley et al. 2008), and the UVOT grism spectra show an indication of Mg II emission (Immler et al. 2008a). Discovered near maximum light, the UV and optical light curves all fade steeply and then shallower and then steeper again. The UVOT light curves will be studied in more detail in M. Modjaz et al. (2009, in preparation). SN 2007Y, a peculiar Ib with spectral similarities to SN 2005bf (Folatelli et al. 2007), behaved more like a Ia in shape and color with the UV brightness rising with the optical, peaking a little sooner and fading slightly quicker. It will be analyzed in detail in M. Stritzinger et al. (2009).

3.3. SNe IIP Light Curves

SNe IIP start off very bright and blue. Brightening to a maximum just a few days after explosion, the UV magnitudes then fade rather linearly, with SN 2005cs fading about twice as fast, as visible in either the right panels of Figure 4 or the histogram of the decay rates in Figure 5. The rapid drop in the UV brightness of SNe II is driven by the cooling photosphere and the resulting line blanketing of heavy elements (see Brown et al. 2007a), so the different decay rates could reflect the different cooling rates of the SN photospheres. Dessart et al. (2008) compare the UVOT photometry of SNe II 2005cs and 2006bp with model spectra and demonstrate the usefulness of UV photometry in constraining the extinction and the temporal change in temperature and ionization. The optical brightness remains constant, resulting in a steady reddening with time. The

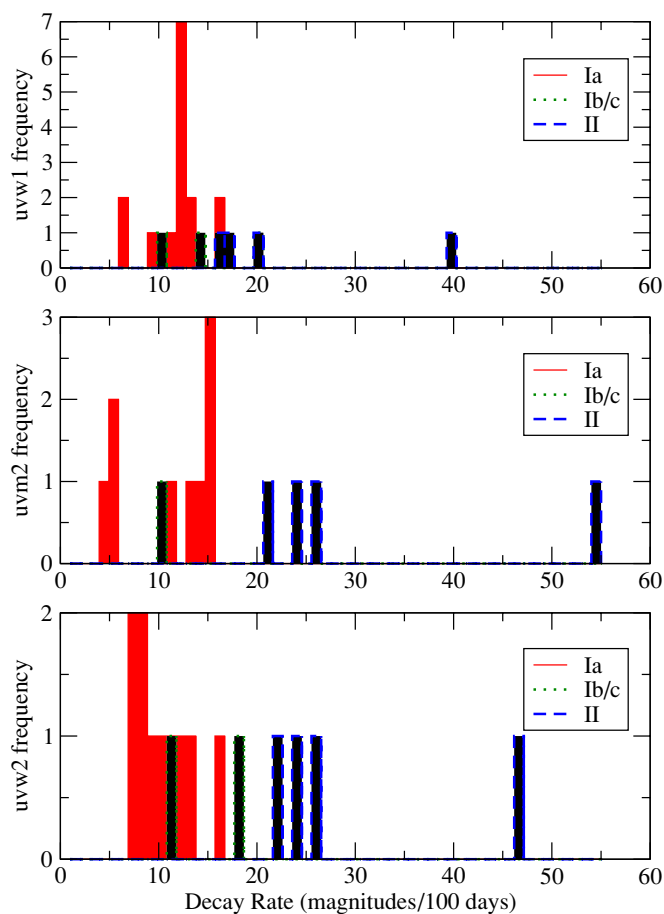


Figure 5. Histogram of the decay rates of the early UV light curves. SNe Ia have very similar decay slopes, particularly in $uvw1$. SNe II decay much faster than SNe Ia and Ib/c, with SN 2005cs decaying twice as fast as the other SNe II.

(A color version of this figure is available in the online journal.)

main SN subtypes missing from our sample are SNe III, II_n, and II_b. Fortunately, examples of these classes—SNe 1979C (Panagia et al. 1980), 1998S (Fransson et al. 2005), and 1993J (Jeffery et al. 1994), along with the peculiar SN II 1987A (Kirshner et al. 1987; Pun et al. 1995)—were well observed with *IUE* and/or *HST*, making these sets complementary. More recent *Swift* observations now include these subtypes as well—SNe 2008es (Miller et al. 2009; Gezari et al. 2009), 2006jd (Immler et al. 2008b), and 2008aq (Brown & Immler 2008).

4. COLORS

In addition to physical properties such as temperature and extinction, UV and UV-optical colors are also useful in differentiating SN types. The use of optical colors to distinguish SNe of different types has been explored by multiple authors (Vanden Berk et al. 2001; Poznanski et al. 2002; Gal-Yam et al. 2004; Sullivan et al. 2006; Kuznetsova & Connolly 2007; Poznanski & Maoz 2007). These techniques are of primary importance for large and deep surveys and searches for which the SN candidates are either too faint or too numerous for spectroscopic classification of all candidates. The upcoming Pan-STARRS could discover on the order of 10,000 SNe/year¹³ and the Large

¹³ <http://pan-starrs.ifa.hawaii.edu/project/reviews/PreCoDR/documents/scienceproposals/sne.pdf>.

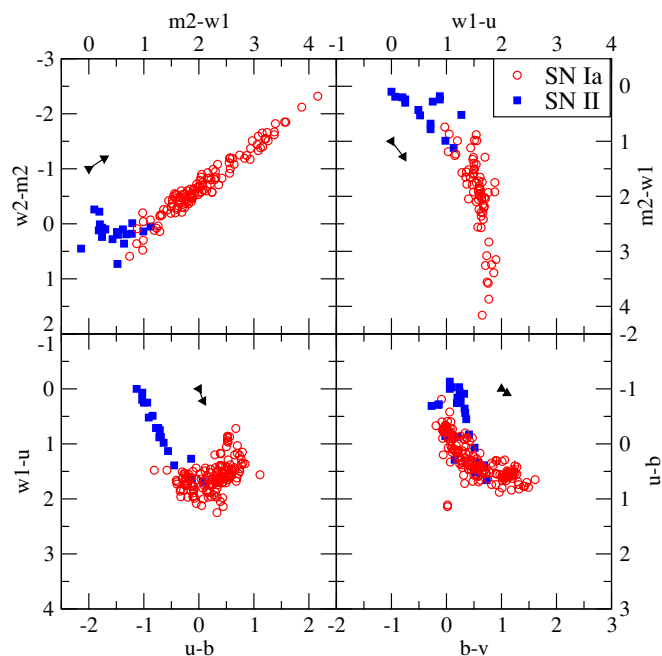


Figure 6. Color-color plots showing the differentiation of young SNe II from SNe Ia. All available colors from all SNe are shown, but the data is trimmed to include only data within 3 mag of the peak in each filter. The ability to differentiate the two increases when the UV and optical regions are sampled, due to the steep red continuum of SNe Ia. The arrows are extinction vectors corresponding to $E(B - V) = 0.1$ computed using the MW extinction relations of Cardelli et al. (1989) evaluated at the central wavelength of the UVOT filters. Note that MW extinction actually causes bluer $uvw2 - uvw1$ colors, rather than the typical “reddening” effect of extinction, due to the $uvw2$ filter coinciding with the 2200 Å bump in the MW extinction curve.

(A color version of this figure is available in the online journal.)

Synoptic Survey Telescope 250,000 SNe/year.¹⁴ Thus photometric measures of the SNe will be critical to classifying SNe, as well as determining photometric redshifts. Rest-frame UV observations can greatly improve the accuracy of such determinations. The clear difference between the UV-bright SNe II and the UV-faint SNe Ia was noticed after a few *IUE* observations of SNe Ia and II (Panagia 1982, see also Panagia 2003). This “UV deficit” is caused by the very red Ia spectrum between ~ 2500 and 4000 Å (see Kirshner et al. 1993), and was exploited by Riess et al. (2004) to identify SNe Ia in the Hubble Deep Field.

Figure 6 compares the color-color location of all appropriate SNe Ia and II data in our sample in five colors (using neighboring filter combinations) available from the UVOT observations. In order to focus on the brighter epochs at which SNe are most likely to be discovered, we have trimmed the data to only include photometry within three magnitudes of the peak (observed or inferred) for that given filter. For SNe Ia this includes about 40 days after maximum light, but only the first ~ 15 days after explosion for an SN II. The UV data for SN 2005cs is supplemented by ground-based *BV* data from Dessart et al. (2008).

Extinction is a complicated issue in the UV, as the effects are strong and varied. The exact extinction vector appropriate for a particular SN would depend on the extinction law, spectral shape (particularly for $uvw2$ and $uvw1$ which have red tails),

¹⁴ http://www.lsst.org/Science/fs_transient.shtml.

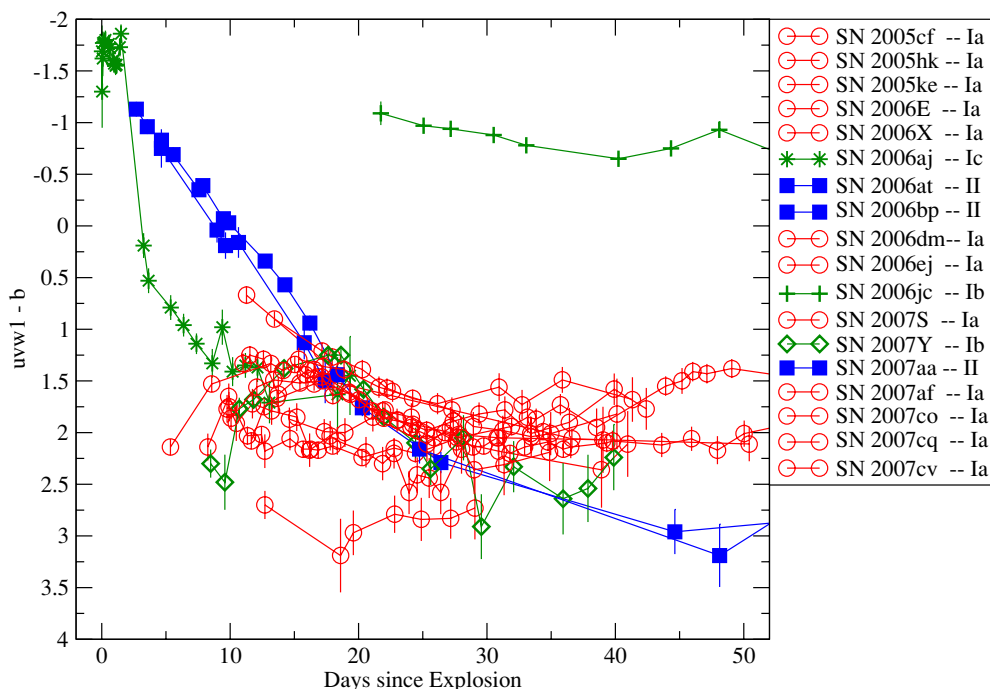


Figure 7. UV-optical color evolution of our sample over the first 50 days. The symbols are the same as used in the above color-color plots. The dramatic color difference at early times vanishes by about 15 days after the explosion.

(A color version of this figure is available in the online journal.)

and total extinction (since the UV reddening becomes non-linear with respect to the optical reddening). To give the general effect of extinction, vectors corresponding to a color excess $E(B - V) = 0.1$ and the Milky Way extinction law (Cardelli et al. 1989) evaluated at the central wavelengths, are plotted in each color-color plot. The SN colors themselves have not been corrected for extinction.

As the UVOT u , b , and v magnitudes are similar to the Johnson UBV , the bottom right panel is comparable to Figure 3 in Poznanski et al. (2002). In those colors there is still a lot of overlap between SNe Ia and II, though SNe II peak 0.5 mag bluer than SNe Ia. With the addition of the $uvw1 - u$ color in the bottom left panel, the bluer SNe II are spread out even more, showing the advantage of rest-frame UV observations. This effect is maximized when a UV filter is combined with an optical filter to sample the spectra slope where SNe II and Ia are most different. There are, however, diminishing returns for colors from neighboring UV filters, as one loses the contrast with the optical light. The best color-color separation (restricting the wavelength range to three consecutive filters) is achieved with $u - b$ and $uvw1 - u$, with young SNe II having colors $uvw1 - u < 1$ and $u - b < -0.5$. As shown below, skipping u to form a $uvw1 - b$ color also differentiates well by itself. In the upper left panel, SNe Ia are actually bluer than SNe II in the $uvw2 - uvw1$ color, but this is likely due to the intrinsic faintness of SNe Ia in the $uvw2$ filter and a combination of the red SN Ia spectral shape and the red tail of the $uvw2$ filter.

While red UV-optical colors differentiate well between young SNe II and Ia, they are not conclusive, as SNe II become redder with time. In Figure 7 we display the $uvw1 - b$ color evolution of these same SNe. At early times, there is a 3 mag difference between the $uvw1 - b$ color of SNe Ia and II, and a color of $uvw1 - b < 1$ includes all of our SNe II less than two weeks old while excluding all Ia data except the earliest epochs of the peculiar SN 2005hk. However, this large difference does not

persist as the SN II temperature and corresponding UV flux drops with time creating a redder spectrum similar to SNe Ia (whose red colors evolve rather slowly) around day 15. Fransson et al. (1987) noticed this rapid reddening in SN 1987A and cautioned against using the UV alone to distinguish SNe I from II. Even a rough determination of the SN epoch, through either the light-curve behavior or even the cadence of the SN search observations can help make the distinction. Reddening is a further degeneracy which can make a young II look older (by about 5 days per additional $E(B - V) \sim 0.2$) or more similar to SNe Ia. This can also be broken by monitoring the color evolution, as reddening would cause a shift in the colors at a given epoch but not mask the differing slopes of the color evolution.

To the color evolution plot we have added the colors of our three SNe Ib/c, spanning the range of colors seen in SNe Ia and II, complicating their differentiation. The similarities of SN 2006jc with SNe II (Pastorello et al. 2008) explains the blue UV-optical colors. SN 2006aj had a bright blue peak and then became very red during the SN bump as was SN 2007Y. SNe Ib/c typically have low effective temperatures and the subsequent UV line blanketing make their colors more similar to SNe Ia. The contamination of SNe Ib/c from cosmological samples of SNe Ia, as discussed in Riess et al. (2004), is reduced because the SNe Ib/c are less common and usually much fainter than SNe Ia.

Understanding the UV color differences within and across types is especially important for classifying high-redshift SNe. Some UV information is being incorporated into such phototyping (see Riess et al. 2004; Johnson & Crots 2006) but in the past has been limited due to the limited epochs at which UV information is available. The addition of this UV photometry should help improve the understanding of the diversity and temporal change of the UV flux to allow SNe to be better identified at larger redshifts. Other high-redshift applications are discussed below.

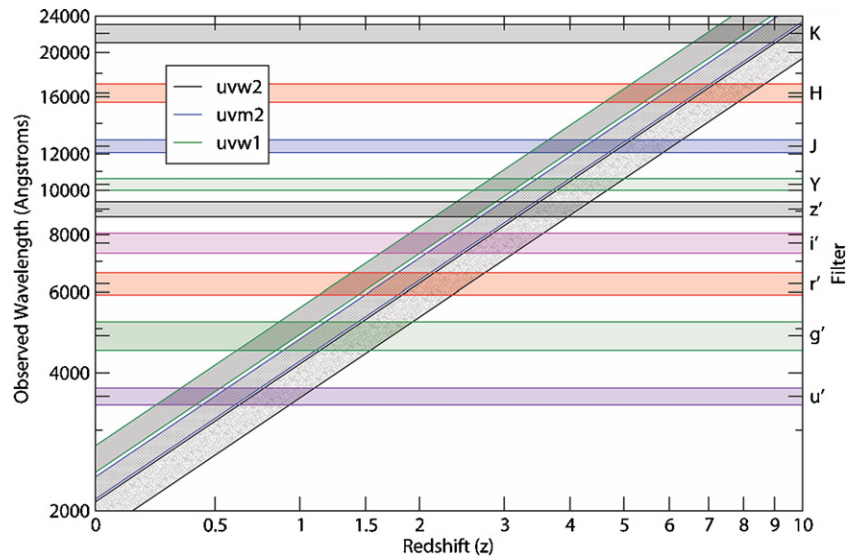


Figure 8. Rest-frame UV light sampled by the UVOT UV filters as it corresponds to observed wavelengths as a function of redshift. The observed wavelength ranges for commonly used filter sets (optical–SDSS (Fukugita et al. 1996) and infrared–UKIRT set (Hewett et al. 2006)) are also highlighted (and labeled on the right side). (A color version of this figure is available in the online journal.)

5. HIGH-REDSHIFT APPLICATION

In addition to SN observations by UV satellites, deep optical observations will observe the rest-frame UV light from higher redshift SNe. Figure 8 displays the rest-frame UV light sampled by the UVOT UV filters as it corresponds to observed wavelengths as a function of redshift, highlighting regions where the UV filters correspond well with commonly used optical and infrared filters. To highlight the regions where the overlap between the filters is greatest, the bands are centered on the central wavelength and extend one quarter of the full width half max of the filter transmission in both directions (Poole et al. 2008; Fukugita et al. 1996; Hewett et al. 2006). This graphically depicts useful regions of overlap. For example, the photons corresponding with the rest-frame *uvw1* begins to be redshifted into the optical *u'* band (e.g., SDSS-II SN survey; Sako et al. 2008; and LSST) for objects at a redshift of $z \sim 0.4$ and the *g'* band (e.g., SNLS; Astier et al. 2006) at $z \sim 0.8$, where the *u' – g'* colors also correspond well with our *uvw2 – uvw1* colors. While chasing the optical light to high redshifts will require observing into the infrared, the use of rest-frame UV light can be done with optical and near-IR observations possible with current and planned large ground-based telescopes.

Aldering et al. (2006) discuss many uses for rest-frame UV observations of these high-redshift SNe in the context of SNAP, and this local sample should allow a comparison looking for evolutionary effects. Since SNAP is planned to have logarithmically spaced filters beginning at 4000 Å, they will cover the rest-frame UV observed by the UVOT filters for redshifts beyond $z \sim 0.8$. More generally, any deep SN search optimized for finding and following high-redshift SNe in the optical will likely also detect the rest-frame UV light of SNe (preferentially SNe II due to their brighter UV luminosities) at the high end of their target redshift and beyond. Measuring SN rates at higher redshifts is only one of many uses of these high-redshift detections. Making full use of this data will require a better understanding of the UV light best obtained for nearby SNe for which multi-wavelength photometry and spectroscopy over a larger portion of the light curve is possible. Rest-frame UV observations of a local sample of SNe have the

further advantage of being a comparison sample with which to understand the high-redshift SNe, look for evolutionary differences (see, e.g., Foley et al. 2008; Ellis et al. 2008), and further constrain photometric redshifts, extinction, and luminosity distances.

6. FUTURE WORK

We have presented here the largest collection of UV light curves obtained by any single instrument, which have allowed the study of individual objects as well as comparisons within and across SN types. In addition to these apparent magnitudes, we are also working to calibrate the absolute magnitudes to many of these objects (P. J. Brown et al., 2009 in preparation). The absolute magnitudes can be used to study the utility of rest-frame UV observations for cosmological measurements and for determining high-redshift SN rates. We are also combining this data with optical and near-infrared observations to construct bolometric light curves that encompass more of the spectrum for individual objects and refining bolometric corrections used in constructing bolometric curves from optical data alone (see Contardo et al. 2000). The light-curve shapes and colors of our large sample should also help in the classification of SNe, particularly at higher redshifts when spectra are unobtainable and fewer rest-frame optical bands are observable. Future UV observatories, including a refurbished *HST*, TAUVE (Safonova et al. 2007), WSO-UV (Pagano et al. 2008) and others, as well as optical observatories observing the high-redshift universe, can also benefit from these light curves to better understand and plan effective UV SN observations.

This work made use of public data from the *Swift* data archive. This work is supported at Penn State by NASA Contract NAS5-00136 and *Swift* Guest Investigator grant NNH06ZDA001N.

REFERENCES

- Aldering, G., Kim, A. G., Kowalski, M., Linder, E. V., & Perlmutter, S. 2007, *Astropart. Phys.*, **27**, 213
 Astier, P., et al. 2006, *A&A*, **447**, 31

- Blustin, A. J. 2007, *Phil. Trans. R. Soc.*, **365**, 1263
- Brown, P. J., & Immler, S. 2008, *ATEL*, **1403**
- Brown, P. J., et al. 2005, *ApJ*, **635**, 1192
- Brown, P. J., et al. 2007a, *ApJ*, **659**, 1488
- Brown, P. J., Roming, P. W. A., Vanden Berk, D. E., Holland, S. T., Immler, S., & Milne, P. A. 2007b, in AIP Conf. Proc. 937, SUPERNOVA 1987A: 20 YEARS AFTER: Supernovae and Gamma-Ray Bursters, ed. S. Immler & K. Weiler (New York: AIP), **386**
- Bufano, F., et al. 2009, *ApJ*, submitted
- Campana, S., et al. 2006, *Nature*, **442**, 1008
- Cappellaro, E., Turatto, M., & Fernley, J. 1995, in IUE-ULDA Access Guide No. 6: Supernovae (ESA-SP 1189; Noordwijk: ESA Publications Division)
- Cardelli, J. A., Clayton, G. C., & Mathis, J. S. 1989, *ApJ*, **345**, 245
- Contardo, G., Leibundgut, B., & Vacca, W.D. 2000, *A&A*, **359**, 876
- Dessart, L., et al. 2008, *ApJ*, **675**, 644
- Ellis, R. S., et al. 2008, *ApJ*, **674**, 51
- Foley, R. J., et al. 2008, *ApJ*, **684**, 68
- Folatelli, G., Morrell, N., Phillips, M., & Hamuy, M. 2007, *CBET*, **862**
- Fransson, C., Grewing, M., Cassatella, A., Panagia, N., & Wamsteker, W. 1987, *A&AL*, **177**, 33
- Fransson, C., et al. 2005, *ApJ*, **622**, 991
- Fukugita, M., Ichikawa, T., Gunn, J. E., Doi, M., Shimasaku, K., & Schneider, D. P. 1996, *AJ*, **111**, 1748
- Gal-Yam, A., Poznanski, D., Maoz, D., Filippenko, A. V., & Foley, R. J. 2004, *PASP*, **116**, 597
- Gal-Yam, A., et al. 2008, *ApJ*, **685**, L117
- Garg, A., et al. 2007, *AJ*, **133**, 403
- Gehrels, N., et al. 2004, *ApJ*, **611**, 1005
- Gezari, S., et al. 2009, *ApJ*, **690**, 1313
- Ghisellini, G., Ghirlanda, G., & Tavecchio, F. 2007, *MNRAS*, **382**, L77
- Hewett, P. C., Warren, S. J., Leggett, S. K., & Hodgkin, S. T. 2006, *MNRAS*, **367**, 454
- Holland, S. T., Immler, S., Brown, P. J., Roming, P. W. A., Vanden Berk, D., & Milne, P. A. 2007, in AIP Conf. Proc. 937, SUPERNOVA 1987A: 20 YEARS AFTER: Supernovae and Gamma-Ray Bursters, ed. S. Immler, & K. Weiler (New York: AIP), **391**
- Holm, A. V., Wu, C., & Caldwell, J. J. 1974, *PASP*, **86**, 296
- Immler, S., et al. 2005, *ApJ*, **632**, 283
- Immler, S., et al. 2006, *ApJ*, **648**, L119
- Immler, S., et al. 2007, *ApJ*, **664**, 435
- Immler, S., et al. 2008a, *ApJL*, **674**, 85
- Immler, S., Brown, P. J., Filippenko, A. V., & Pooley, D. 2008b, *ATEL*, **1290**
- Jeffery, D. J., et al. 1994, *AJ*, **421**, L27
- Johnson, B. D., & Crots, A. P. A. 2006, *AJ*, **132**, 756
- Kasliwal, M. 2008, *ApJ*, **683**, L29
- Kirshner, R. P., Sonneborn, G., Crenshaw, D. M., & Nassiopoulos, G. E. 1987, *ApJ*, **320**, 602
- Kirshner, R. P., et al. 1993, *ApJ*, **415**, 589
- Kuznetsova, N. V., & Connolly, B. M. 2007, *ApJ*, **659**, 530
- Lentz, E. J., Baron, E., Branch, D., Haushildt, P. H., & Nugent, P. E. 2000, *ApJ*, **530**, 966
- Li, W., Jha, S., Filippenko, A. V., Bloom, J. S., Pooley, D., Foley, R. J., & Perley, D. A. 2006, *PASP*, **118**, 37
- Lyubimkov, L. S. 1990, *SvA*, **34**, 239
- Miller, A. A., et al. 2009, *ApJ*, **690**, 1303
- Milne, P. A., Brown, P. J., Holland, S. T., Roming, P. W. A., & Immler, S. 2007, in AIP Conf. Proc. 937, SUPERNOVA 1987A: 20 YEARS AFTER: Supernovae and Gamma-Ray Bursters, ed. S. Immler & K. Weiler (New York: AIP), **303**
- Modjaz, M., et al. 2006, *ApJL*, **645**, 21
- Modjaz, M., et al. 2008, *ApJ*, submitted (arXiv:0805.2201)
- Nugent, P., et al. 1997, *ApJ*, **485**, 812
- Pagano, I., et al. 2008, arXiv:0801.2039
- Panagia, N. 1982, Proc. 3rd European IUE Conf. (ESA SP-176; Noordwijk: ESA Publications Division), **31**
- Panagia, N. 2003, in Lecture Notes in Physics Vol. 598, Supernovae and Gamma-Ray Bursters, ed. K. Weiler (Berlin: Springer), **113**
- Panagia, N., et al. 1980, *MNRAS*, **192**, 861
- Pastorello, A., et al. 2008, *MNRAS*, **389**, 113
- Phillips, M. M., et al. 2007, *PASP*, **119**, 360
- Pian, E., et al. 2006, *Nature*, **442**, 1011
- Poole, T., et al. 2008, *MNRAS*, **383**, 627
- Poznanski, D., Gal-Yam, A., Maoz, D., Filippenko, A. V., Leonard, D. C., & Matheson, T. 2002, *PASP*, **114**, 833
- Poznanski, D., & Maoz, D. 2007, *AJ*, **134**, 1285
- Pskovskii, U. P. 1967, *SvA*, **11**, 63
- Pun, C. S. J., et al. 1995, *ApJS*, **99**, 223
- Riess, A. G., et al. 2004, *ApJ*, **600**, L163
- Roming, P. W. A., et al. 2005, *Space Sci. Rev.*, **120**, 95
- Safonova, M., Sivaram, C., & Murthy, J. 2008, *Ap&SS*, **318**, 1
- Sako, M., et al. 2008, *AJ*, **135**, 348
- Sauer, D. N., et al. 2008, *MNRAS*, **391**, 1605
- Stritzinger, M., et al. 2002, *AJ*, **124**, 2200
- Stritzinger, M., et al. 2009, *ApJ*, accepted, arXiv:0902.0609
- Sullivan, M., et al. 2006, *AJ*, **131**, 960
- Vanden Berk, D. E., et al. 2001, *BAAS*, **199**.8405
- Wang, L., Aldering, G., Filippenko, A. V., Challis, P., Nugent, P., Li, W., Matheson, T., & Howell, A. 2005, *BAAS*, **206**.4501
- Wang, X., et al. 2008, *ApJ*, **675**, 626
- Wang, X., et al. 2009, *ApJ*, submitted (arXiv:0811.1205)
- Waxman, E., Meszaros, P., & Campana, S. 2007, *ApJ*, **667**, 351